Flux-Controlled Two-Site Kitaev Chain

Kulesh, Ivan; Ten Haaf, Sebastiaan L.D.; Wang, Qingzhen; Sietses, Vincent P.M.; Zhang, Yining; Roelofs, Sebastiaan R.; Prosko, Christian G.; Xiao, Di; Goswami, Srijit; More Authors

DOI
10.1103/r9pv-2prs

Publication date
2025

Document Version
Final published version

Published in
Physical review letters

Editors' Suggestion

Flux-Controlled Two-Site Kitaev Chain

Ivan Kulesh,[1,*] Sebastiaan L. D. ten Haaf,[1,*] Qingzhen Wang,[1] Vincent P. M. Sietses,[1] Yining Zhang,[1] Sebastiaan R. Roelofs,[1] Christian G. Prosko,[1] Di Xiao,[2] Candice Thomas,[2] Michael J. Manfra,[2,3,4] and Srijit Goswami[1,†]

[1]*QuTech and Kavli Institute of Nanoscience, Delft University of Technology, Delft, 2600 GA, The Netherlands*
[2]*Department of Physics and Astronomy, Purdue University, West Lafayette, Indiana 47907, USA*
[3]*School of Materials Engineering, Purdue University, West Lafayette, Indiana 47907, USA*
[4]*Elmore School of Electrical and Computer Engineering, Purdue University, West Lafayette, Indiana 47907, USA*

(Received 5 February 2025; accepted 7 July 2025; published 30 July 2025)

In semiconducting-superconducting hybrid devices, Andreev bound states (ABSs) can mediate the coupling between quantum dots, allowing for the realization of artificial Kitaev chains. In order to engineer Majorana bound states (MBSs) in these systems, one must control the energy of the ABSs. In this Letter, we show how extended ABSs in a flux-tunable Josephson junction can be used to control the coupling between distant quantum dots separated by $\simeq 1$ μm. In particular, we demonstrate that the combination of electrostatic control and phase control over the ABSs increases the parameter space in which MBSs are observed. Finally, by employing an additional spectroscopic probe in the hybrid region between the quantum dots, we gain information about the spatial distribution of the Majorana wave function in a two-site Kitaev chain.

DOI: 10.1103/r9pv-2prs

Introduction—Quantum dots (QDs) with an induced superconducting (SC) coupling can be used to create solid-state quantum entanglers [1–5] as well as to implement quantum gates for spin qubits [6,7]. Moreover, QDs with both a superconducting coupling and a hopping interaction offer a platform for constructing an artificial Kitaev chain [8,9], hosting Majorana bound states (MBSs). The minimal chain is a system of two QDs, which can be tuned to host so-called poor man's Majoranas (PMMs) [10,11]. While not topologically protected from perturbations, these states are expected to exhibit Majorana properties, such as non-Abelian exchange statistics [12,13]. A crucial prerequisite to implement a PMM is the ability to control the coupling between spin-polarized QDs. It was demonstrated that a proximitized semiconducting-superconducting hybrid region, hosting Andreev bound states (ABSs), is an excellent mediator to couple the QDs [14–17]. The nature and magnitude of this coupling can be tuned by changing the electrostatic potential of the hybrid region as well as by changing the orientation of the external magnetic field [15,16]. Both were recently explored in experiments demonstrating the realization of the PMM states [18,19].

Here, we further explore the role of ABSs in realizing PMM states by exploiting a novel geometry in a two-dimensional electron gas (2DEG) hybrid system. Motivated by recent theory work [20], we utilize ABSs coupled to two SC electrodes embedded in a loop, such that the phase difference between the electrodes can be controlled with an applied perpendicular magnetic field. Taking advantage of the long coherence length of the 2DEG, we are able to couple QDs separated by about 1 μm. We observe that the superconducting phase difference changes the effective coupling between two QDs and allows for finding PMM sweet spots within a continuous range of the ABS chemical potential. This is an improvement on systems without this phase control, where sweet spots arise only at two discrete points of the ABS chemical potential [14,15]. Despite the relatively large separation of the two QDs, an induced interdot coupling on the order of $10-30$ μeV is extracted from the spectroscopic measurements. This demonstrates a clear advantage of using ABSs in proximitized semiconductors for providing a long-range coupling between QDs and relaxes spatial restrictions on PMM-device design. Lastly, exploiting the flexible 2DEG architecture, we utilize a spectroscopic probe connected to the proximitized ABS segment. This additional probe allows us to study the spatial distribution of the PMM wave functions in the strongly coupled regime [21].

Device design and characterization—The device is implemented on an InSbAs two-dimensional electron gas capped with 7 nm epitaxial aluminum [22]. Operating in depletion mode, the first layer of gates [red, Figs. 1(a) and 1(b)] define a one-dimensional channel connected to three spectroscopy terminals (yellow). Voltages are applied to the plunger gates (blue), with V_{QDL} and V_{QDR} tuning the

*These authors contributed equally to this work.
†Contact author: S.Goswami@tudelft.nl

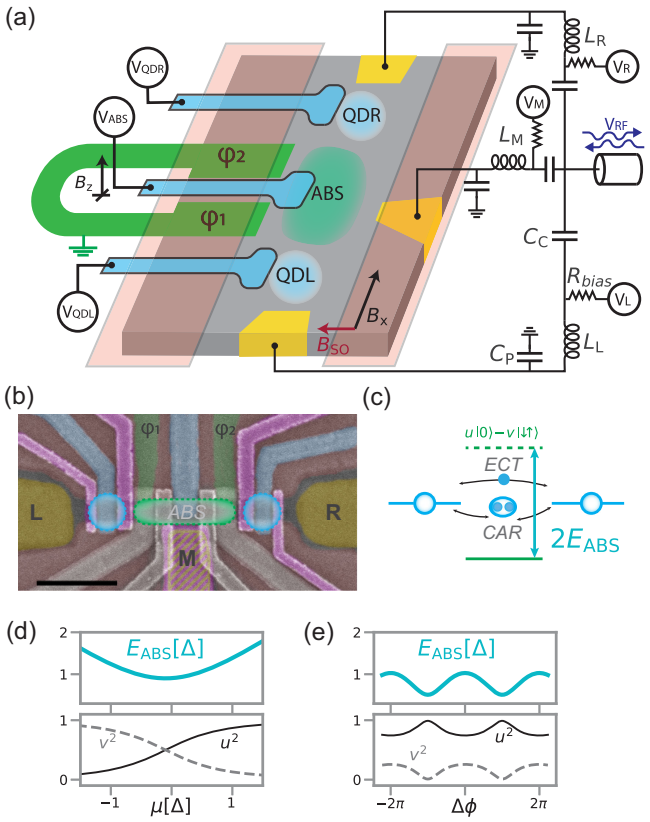

FIG. 1. Schematic of the device measured (a) and false-colored SEM image (b): a grounded superconducting loop (green) is used to create a phase difference between two terminals ϕ_1 and ϕ_2, extending into the ABS region in a one-dimensional channel, formed by two depletion gates (red). Plunger gates (blue) are used to control QDs and ABS chemical potential. Three normal spectroscopic terminals (yellow) are connected to resonators, formed by off-chip coil inductors L_X and the parasitic capacitances of bond wires C_P, with coupling capacitors C_C allowing for a multiplexed readout. Cutter gates [pink, shown only in (b)] are used to confine quantum dots and define tunnel barriers. Terminal M is situated beneath the corresponding cutter gate. The scale bar in (b) is 500 nm. A zoomed-out image of a similar device can be found in [23]. The experiment is shown schematically in (c): ABS (green) mediates ECT and CAR between quantum dots. The amplitudes of those nonlocal processes depend on the ABS energy E_{ABS} and its coherence factors u and v, which, in turn, can be controlled by either the ABS chemical potential μ (d) or the phase difference $\Delta\phi$ (e). Energy is in units of induced SC pairing amplitude in the atomic limit.

respective QDs' chemical potentials, while V_{ABS} controls the chemical potential of the hybrid region. The plunger gates and the tunnel gates (purple) are situated in the second and third layers. A similar device architecture has been used in a three-site configuration [23].

Two superconducting terminals (green) are connected in a loop and protrude into the channel, establishing an extended proximitized region. The superconducting loop is kept grounded, so that an out-of-plane field B_z controls the phase difference $\Delta\phi = \phi_2 - \phi_1$ between the two SC electrodes. Measurements are performed using subgigahertz off-chip resonators, which are connected to the corresponding tunnel probes (see Supplemental Material [24] for schematics). The resonators can be probed simultaneously using a multiplexed reflectometry setup [25]. The complex reflected rf signal of each lead $X \in \{L, M, R\}$ resonator is converted to the single real value $\tilde{V}_{rf}^{X}$ by performing a rotation in the complex plane [24]. This signal is representative of the device conductance [26–28]. Each resonator is connected to a bias tee R_{bias}, allowing for applying a bias voltage to each spectroscopic normal lead as well as for measuring the flow of current through each lead. This additionally allows extracting the device conductance $G_{xx} = dV_x/dI_x$ using a standard low-frequency lock-in technique. The measurements are performed in a dilution refrigerator with a base temperature of 20 mK.

The QDs are coupled by a hopping interaction through elastic cotunneling (ECT) and by a pairing interaction arising from crossed Andreev reflection (CAR), schematically illustrated in Fig. 1(c). The amplitudes of both these nonlocal processes depend on the ABS energy E_{ABS} [14]. Additionally, ECT and CAR respond differently to the charge character of the ABS (determined by the coherence factors u and v). Thus, when varying the ABS parameters with either the chemical potential μ or the phase $\Delta\phi$ [schematically illustrated in Figs. 1(d) and 1(e) for an atomic limit model], one expects to be able to control the ECT to CAR ratio [20].

To mediate ECT and CAR between the distant QDs, an ABS is required that extends throughout the entire hybrid region in between them. We first establish the presence of such an extended state in this device, particularly considering the relatively large length of this region—700 nm (distance between innermost cutter gates), comparable to the SC coherence length in similar systems [29,30]. This is achieved by performing tunneling spectroscopy measurements from three sides (left, middle, and right), where we energize only the three barriers, adjacent to the ABS [Fig. 2(a)]. We separately vary either the ABS chemical potential by changing the voltage V_{ABS} or the phase $\Delta\phi$ by applying a magnetic field B_z. We observe that the spectrum shows a correlated dependence from all three terminals, as a function of both gate voltage [Fig. 2(b)] and magnetic field [Fig. 2(c)], implying that a single quantum state is accessible to both quantum dots.

Tuning into PMM regime—Having established the presence of extended ABSs in our device, we proceed with forming the PMM system. First, we energize the additional outermost gates to define the QDs. An in-plane magnetic field $B_x = 150$ mT is applied, in order to spin polarize the QDs. To achieve strong coupling between the QDs, the innermost gates are set to have relatively high tunneling between the QDs and the hybrid region [21,31]. In this regime, the QDs are commonly described as

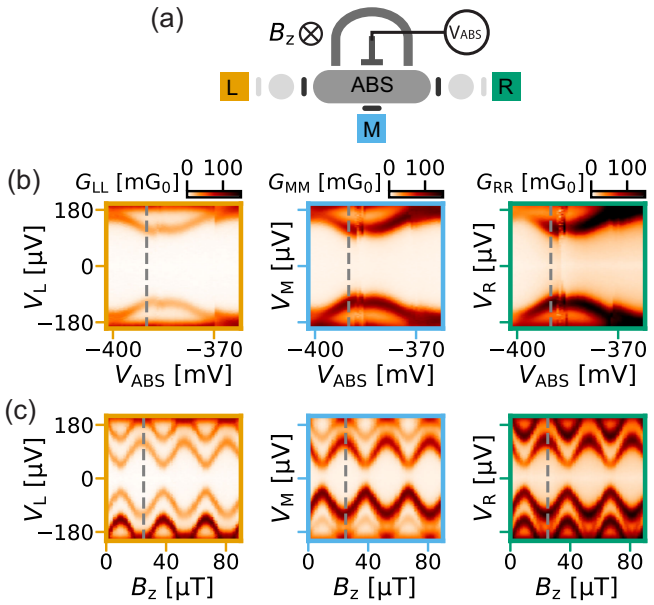

FIG. 2. Schematic of the device with three tunneling spectroscopy terminals used to probe an extended ABS (a). For these measurements, only the three barrier gates adjacent to the ABS region are energized. Top panel (b): tunneling spectroscopy measurements acquired while varying the ABS chemical potential. Bottom panel (c): tunneling spectroscopy measurements, varying the out-of-plane field threading the SC loop. Corresponding fixed V_{ABS} and B_z values are indicated by the dashed lines in (b) and (c). For both panels, we plot lock-in conductance $G_{XX} = dV_X/dI_X$. The periodicity in field (28 μT) agrees well with the loop area (60 μm^2). Both measurements are performed at zero in-plane magnetic field.

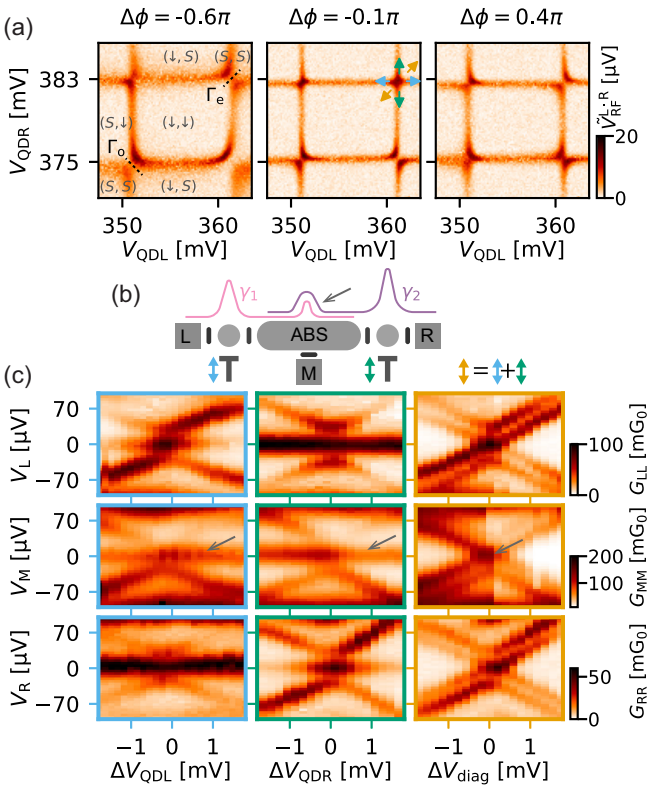

FIG. 3. Tuning into the PMM sweet spot and verifying the PMM spectrum. Top panel (a): charge stability diagrams, shown in correlated voltage $\tilde{V}_{rf}^{L,R} = \sqrt{\tilde{V}_{rf}^{L} \cdot \tilde{V}_{rf}^{R}}$ (each component measured from the Coulomb blockade [24]), varying the superconducting phase difference $\Delta\phi(B_z)$. Combined QD states are indicated in brackets. States coupled by Γ_o (Γ_e) are connected with the dashed lines. (b) Schematic of the detuning experiment, showing PMM wave functions γ_1 and γ_2, which can reside partially in the ABS region. (c) Tunneling spectroscopy, measured with a lock-in from all three probes, plotted in conductance G_{XX}. Note the signal at zero bias measured at the middle probe, highlighted with the arrows. V_{ABS} is fixed at −420 mV.

Yu-Shiba-Rusinov states [32–36], as observed in spectroscopy measurements [24]. Depending on the dot chemical potential, the ground state of each QD is either a $|\downarrow\rangle$ doublet or a singlet $|S\rangle$ superposition of the empty and double-occupied QD state. With this description of the QD states, the simple picture of ECT and CAR interactions can be extended. Considering the combined state of the two QDs, two types of effective interactions can be defined [19,21]: spin-conserving Γ_o, coupling $|S,\downarrow\rangle$ with $|\downarrow, S\rangle$, and spin-nonconserving Γ_e, which couples $|\downarrow,\downarrow\rangle$ with $|S, S\rangle$; see Fig. 3(a). Notably, those quantities can be expressed via ECT and CAR amplitudes t and Δ. Thus, Γ_o is a linear combination of spin-conserving terms $t_{\downarrow\downarrow}$, $t_{\uparrow\uparrow}$, $\Delta_{\uparrow\downarrow}$, and $\Delta_{\downarrow\uparrow}$ (note that the CAR couples opposite spins), while Γ_e can be expressed via spin-flipping terms $t_{\uparrow\downarrow}$, $t_{\downarrow\uparrow}$, $\Delta_{\uparrow\uparrow}$, and $\Delta_{\downarrow\downarrow}$. Without the spin-orbit interaction present, or when the external magnetic field is applied alongside the spin-orbit field B_{SO}, only Γ_o is significant. Therefore, we apply the in-plane magnetic field alongside the dot-dot axis, perpendicular to the direction of the B_{SO} (see Ref. [24]).

The different types of couplings between the QDs are revealed in charge stability diagrams (CSDs), obtained by sweeping the QD plunger voltages and measuring reflected rf signals from the left and right normal leads [Fig. 3(a)]. We record the CSDs while varying B_z, which can be converted to the phase difference $\Delta\phi$ across SC electrodes (we assign $\Delta\phi = 0$ to the point of maximum E_{ABS} [24]). Measured avoided crossings demonstrate the $\Gamma_o(\Gamma_e)$ coupling dominating, depending on whether the avoided crossing is (anti)diagonal. In this example, we observe that varying $\Delta\phi$ indeed can change the coupling regime from $\Gamma_e > \Gamma_o$ to $\Gamma_e < \Gamma_o$ for the top-right transition, with the modulation being 2π periodic in $\Delta\phi$ [24]. This ability to change the coupling regime with the phase difference originates from the fact that $\Delta\phi$ affects the ABS coherence factors u and v (Fig. 1), contributing in a different manner to ECT and CAR [14,20] and, consequently, to Γ_e and Γ_o. Moreover, the presence of the Zeeman field and the spin-orbit interaction in the proximitized region further affects

the interplay between $\Delta\phi$ and the spin-split ABS spectrum [37–39], additionally affecting the spin-conserving (-flipping) ECT $t_{\sigma_1\sigma_2}$ and CAR $\Delta_{\sigma_1\sigma_2}$ amplitudes [15].

The point where $\Gamma_e = \Gamma_o$ corresponds to the so-called PMM sweet spot [19,21], with the dot transitions crossing in straight lines. We proceed to verify the sweet spot conditions by performing the spectroscopy measurements [Figs. 3(b) and 3(c)] while detuning either one or both QDs. As expected [10], the zero-bias conductance peak persists when detuning only one QD and splits from zero energy when detuning both QDs. The minimum energy of the excited states allows for estimating the coupling amplitudes to be on the order of 18 μV (and up to 30 μV for the regime described in Supplemental Material [24]). This is comparable to previously reported values [19,31], indicating that the increased length of the ABS segment does not significantly impact the interaction strength. Leveraging the flexibility of the 2DEG platform, we utilize the spectroscopic probe of the ABS region to study the PMM wave function profile in the device. As shown in Fig. 3(c), we find that a zero-bias conductance peak is also clearly visible in the conductance G_{MM}. This is an indication that the PMM wave functions γ_1 and γ_2 both reside partially in the ABS region, such that electron transfer from the lead M to the delocalized zero-energy fermionic mode is possible. Operating in the strong coupling regime, a finite overlap of the PMM wave functions inside the ABS segment is expected [20,21], since the ABS does not constitute a "bulk" site, unlike the middle dot in a three-site Kitaev chain [23]. Importantly, we find that, despite this overlap, we can still detune the dots while preserving the zero-energy states. As expected from the theory, the relevant metric to exploit PMM physics is the overlap on the outer QDs [13,20,21].

Exploring the gate-phase parameter space—The section above demonstrates that the relative amplitudes of Γ_e and Γ_o couplings can be accurately controlled through controlling the superconducting phase difference. Now, we proceed to explore how this can be used to complement the previously established control utilizing the ABS chemical potential [15,16,18]. As with phase, this tunability is achieved through the dependence of the ABS energy E_{ABS}, as well as the coherence factors u and v, on ABS gate voltage [14]. Moreover, one expects that the dependence of the ABS parameters on the phase difference $\Delta\phi$ is modified when varying the ABS chemical potential μ [20]. Qualitatively, this can be pictured as the junction transparency being a function of μ. This further motivates us to explore the two-dimensional V_{ABS}, $\Delta\phi$ parameter space. The results of this experiment are summarized in Fig. 4. We record CSDs, focusing on a specific transition [corresponding to the top right in Fig. 3(a)], while varying $\Delta\phi(B_z)$. Comparing these CSDs for different V_{ABS}, we observe that a PMM sweet spot, corresponding to the crossover between dominant Γ_e to Γ_o, can be obtained for each V_{ABS} set point

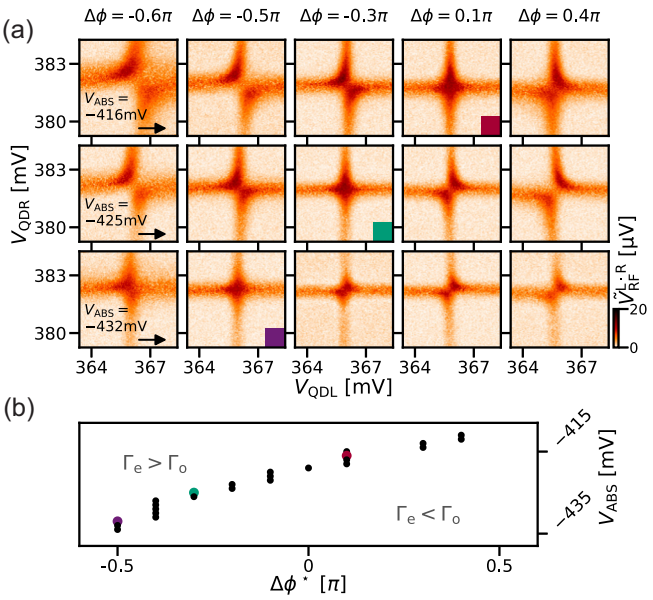

FIG. 4. The sweet spot location in the ABS gate–SC phase difference space. We capture charge stability diagrams (a) for a set of fixed V_{ABS} voltages while varying $\Delta\phi$. The sweet spot $\Delta\phi^*$ is then determined for each V_{ABS} as a crossover between Γ_o and Γ_e, corresponding to the straight QD charge transition lines and marked with a colored square. We repeat this procedure for multiple V_{ABS} values and plot the extracted $\Delta\phi^*$ in (b).

in this range. Moreover, small changes in the V_{ABS} result in a small change of the sweet spot phase difference $\Delta\phi^*$. This demonstrates that, for a certain $\Delta\phi$, V_{ABS} range, the PMM sweet spot spans a continuous line in a two-dimensional space. Without the phase control, the explored V_{ABS} range would contain only a single sweet spot, as shown in previous works on two-site chains [18,19]. It is predicted that the sweet spot characteristics, such as the excitation gap, change systematically alongside $\Gamma_e = \Gamma_o$ line in the $\Delta\phi$, V_{ABS} plane. However, we have not observed any such systematic behavior, exploring multiple regimes throughout several device cooldowns (see Supplemental Material [24]). This discrepancy with the theoretical predictions [20] can be attributed to the presence of multiple states in the proximitized region [Fig. 2(c)] as well as the spin splitting of said states.

Conclusions—We have demonstrated the possibility of strongly coupling two QDs via an extended Andreev bound state in a proximitized InSbAs 2DEG on a 700-nm-long hybrid segment. Obtained coupling amplitudes are on the same order of magnitude as reported in preceding studies [18,19] with short (150–200 nm) hybrid segments, thus relaxing constraints for future designs. We found that embedding the hybrid region in a SC loop allows for a novel control knob over the effective ECT and CAR couplings between the two QDs with the superconducting phase difference. Here, we explored the phase control to tune the system to a set of sweet spots hosting PMM states.

Combined with control through the ABS chemical potential established in previous works, we found that sweet spots can be obtained along a continuous path in the gate-phase space. As such, it can be utilized to avoid electrostatically unstable gate regions. Future studies can benefit from dedicated flux lines to control the interaction between QDs, which may reduce gate cross-coupling and enhance charge stability when compared with the electrostatic gate control. Lastly, we studied the PMM wave functions in the ABS segment and observed their presence in tunneling spectroscopy, suggesting the states are not fully localized on the QDs. Moreover, the middle probe allows for the *in situ* monitoring of the ABS spectrum while tuning into a PMM regime. These results expand the device geometry and support the understanding of coupled quantum dots in a PMM system. Our design can be of interest for realizing a long-range tunable superconducting coupling for spin-qubit architectures [6,7,40,41], not reliant on the usage of multidot chains [42] or coupling cavities [43].

Acknowledgments—The authors thank O. W. B. Benningshof and J. D. Mensingh for technical assistance with the cryogenic electronics. The authors are grateful to Juan Daniel Torres Luna and Chun-Xiao Liu for helpful discussions. The research was supported by the Dutch National Science Foundation (NWO), Microsoft Corporation Station Q, and a grant from Top consortium for Knowledge and Innovation program (TKI). S. G. acknowledges financial support from the Horizon Europe Framework Program of the European Commission through the European Innovation Council Pathfinder Grant No. 101115315 (QuKiT).

The device was fabricated by Q. W. using a 2DEG heterostructure provided by D. X., C. T., and M. J. M., while S. L. D. t. H. and I. K. contributed to the device design and fabrication flow optimization. The experiment was devised by I. K. Initial device characterization was performed by Y. Z. Experimental data were obtained by V. P. M. S., supervised by I. K. and S. L. D. t. H. I. K., S. L. D. t. H., V. P. M. S., Y. Z., S. R. R., and C. G. P. designed the measurement setup. I. K. and S. L. D. t. H. wrote the manuscript with input from all authors. S. G. supervised the project.

Data availability—The data that support the findings of this Letter are openly available [44].

[1] P. Recher, E. V. Sukhorukov, and D. Loss, Andreev tunneling, Coulomb blockade, and resonant transport of nonlocal spin-entangled electrons, Phys. Rev. B **63**, 165314 (2001).
[2] N. M. Chtchelkatchev, G. Blatter, G. B. Lesovik, and T. Martin, Bell inequalities and entanglement in solid-state devices, Phys. Rev. B **66**, 161320(R) (2002).
[3] P. Samuelsson, E. V. Sukhorukov, and M. Büttiker, Orbital entanglement and violation of Bell inequalities in mesoscopic conductors, Phys. Rev. Lett. **91**, 157002 (2003).
[4] P. Busz, D. Tomaszewski, and J. Martinek, Spin correlation and entanglement detection in Cooper pair splitters by current measurements using magnetic detectors, Phys. Rev. B **96**, 064520 (2017).
[5] F. Brange, O. Malkoc, and P. Samuelsson, Minimal entanglement witness from electrical current correlations, Phys. Rev. Lett. **118**, 036804 (2017).
[6] M. Leijnse and K. Flensberg, Coupling spin qubits via superconductors, Phys. Rev. Lett. **111**, 060501 (2013).
[7] M. Spethmann, S. Bosco, A. Hofmann, J. Klinovaja, and D. Loss, High-fidelity two-qubit gates of hybrid superconducting-semiconducting singlet-triplet qubits, Phys. Rev. B **109**, 085303 (2024).
[8] A. Y. Kitaev, Unpaired Majorana fermions in quantum wires, Phys. Usp. **44**, 131 (2001).
[9] J. D. Sau and S. D. Sarma, Realizing a robust practical Majorana chain in a quantum-dot-superconductor linear array, Nat. Commun. **3**, 964 (2012).
[10] M. Leijnse and K. Flensberg, Parity qubits and poor man's Majorana bound states in double quantum dots, Phys. Rev. B **86**, 134528 (2012).
[11] A. Tsintzis, R. S. Souto, and M. Leijnse, Creating and detecting poor man's Majorana bound states in interacting quantum dots, Phys. Rev. B **106**, L201404 (2022).
[12] C.-X. Liu, H. Pan, F. Setiawan, M. Wimmer, and J. D. Sau, Fusion protocol for Majorana modes in coupled quantum dots, Phys. Rev. B **108**, 085437 (2023).
[13] A. Tsintzis, R. S. Souto, K. Flensberg, J. Danon, and M. Leijnse, Majorana qubits and non-Abelian physics in quantum dot–based minimal Kitaev chains, PRX Quantum **5**, 010323 (2024).
[14] C.-X. Liu, G. Wang, T. Dvir, and M. Wimmer, Tunable superconducting coupling of quantum dots via Andreev bound states in semiconductor-superconductor nanowires, Phys. Rev. Lett. **129**, 267701 (2022).
[15] A. Bordin, G. Wang, C.-X. Liu, S. L. D. ten Haaf, N. van Loo, G. P. Mazur, D. Xu, D. van Driel, F. Zatelli, S. Gazibegovic, G. Badawy, E. P. A. M. Bakkers, M. Wimmer, L. P. Kouwenhoven, and T. Dvir, Tunable crossed Andreev reflection and elastic cotunneling in hybrid nanowires, Phys. Rev. X **13**, 031031 (2023).
[16] Q. Wang, S. L. D. ten Haaf, I. Kulesh, D. Xiao, C. Thomas, M. J. Manfra, and S. Goswami, Triplet correlations in Cooper pair splitters realized in a two-dimensional electron gas, Nat. Commun. **14**, 4876 (2023).
[17] Z.-H. Liu, C. Zeng, and H. Q. Xu, Coupling of quantum-dot states via elastic cotunneling and crossed Andreev reflection in a minimal Kitaev chain, Phys. Rev. B **110**, 115302 (2024).
[18] T. Dvir, G. Wang, N. van Loo, C.-X. Liu, G. P. Mazur, A. Bordin, S. L. D. ten Haaf, J.-Y. Wang, D. van Driel, F. Zatelli, X. Li, F. K. Malinowski, S. Gazibegovic, G. Badawy, E. P. A. M. Bakkers, M. Wimmer, and L. P. Kouwenhoven, Realization of a minimal Kitaev chain in coupled quantum dots, Nature (London) **614**, 445 (2023).
[19] S. L. D. ten Haaf, Q. Wang, A. M. Bozkurt, C.-X. Liu, I. Kulesh, P. Kim, D. Xiao, C. Thomas, M. J. Manfra, T. Dvir,

M. Wimmer, and S. Goswami, A two-site Kitaev chain in a two-dimensional electron gas, Nature (London) **630**, 329 (2024).

[20] J. D. T. Luna, A. M. Bozkurt, M. Wimmer, and C.-X. Liu, Flux-tunable Kitaev chain in a quantum dot array, SciPost Phys. Core **7**, 065 (2024).

[21] C.-X. Liu, A. M. Bozkurt, F. Zatelli, S. L. D. ten Haaf, T. Dvir, and M. Wimmer, Enhancing the excitation gap of a quantum-dot-based Kitaev chain, Commun. Phys. **7**, 235 (2024).

[22] C. M. Moehle, C. T. Ke, Q. Wang, C. Thomas, D. Xiao, S. Karwal, M. Lodari, V. van de Kerkhof, R. Termaat, G. C. Gardner, G. Scappucci, M. J. Manfra, and S. Goswami, InSbAs two-dimensional electron gases as a platform for topological superconductivity, Nano Lett. **21**, 9990 (2021).

[23] S. L. D. ten Haaf, Y. Zhang, Q. Wang, A. Bordin, C.-X. Liu, I. Kulesh, V. P. M. Sietses, C. G. Prosko, D. Xiao, C. Thomas, M. J. Manfra, M. Wimmer, and S. Goswami, Observation of edge and bulk states in a three-site Kitaev chain, Nature (London) **641**, 890 (2025).

[24] See Supplemental Material at http://link.aps.org/supplemental/10.1103/r9pv-2prs for (i) a description of the device fabrication, (ii) a detailed description of the measurement setup and data processing, and (iii) extended datasets supporting the main text.

[25] J. Hornibrook, J. Colless, A. Mahoney, X. Croot, S. Blanvillain, H. Lu, A. Gossard, and D. Reilly, Frequency multiplexing for readout of spin qubits, Appl. Phys. Lett. **104**, 103108 (2014).

[26] D. Reilly, C. Marcus, M. Hanson, and A. Gossard, Fast single-charge sensing with a rf quantum point contact, Appl. Phys. Lett. **91**, 162101 (2007).

[27] M. Jung, M. Schroer, K. Petersson, and J. R. Petta, Radio frequency charge sensing in InAs nanowire double quantum dots, Appl. Phys. Lett. **100**, 253508 (2012).

[28] D. Razmadze, D. Sabonis, F. K. Malinowski, G. C. Ménard, S. Pauka, H. Nguyen, D. M. T. van Zanten, E. C. T. O' Farrell, J. Suter, P. Krogstrup, F. Kuemmeth, and C. M. Marcus, Radio-frequency methods for Majorana-based quantum devices: Fast charge sensing and phase-diagram mapping, Phys. Rev. Appl. **11**, 064011 (2019).

[29] W. Mayer, J. Yuan, K. S. Wickramasinghe, T. Nguyen, M. C. Dartiailh, and J. Shabani, Superconducting proximity effect in epitaxial Al-InAs heterostructures, Appl. Phys. Lett. **114**, 103104 (2019).

[30] A. M. Whiticar, A. Fornieri, E. C. T. O'Farrell, A. C. C. Drachmann, T. Wang, C. Thomas, S. Gronin, R. Kallaher, G. C. Gardner, M. J. Manfra, C. M. Marcus, and F. Nichele, Coherent transport through a Majorana island in an Aharonov–Bohm interferometer, Nat. Commun. **11**, 3212 (2020).

[31] F. Zatelli, D. van Driel, D. Xu, G. Wang, C.-X. Liu, A. Bordin, B. Roovers, G. P. Mazur, N. van Loo, J. C. Wolff, A. M. Bozkurt, G. Badawy, S. Gazibegovic, E. P. A. M. Bakkers, M. Wimmer, L. P. Kouwenhoven, and T. Dvir, Robust poor man's Majorana zero modes using Yu-Shiba-Rusinov states, Nat. Commun. **15**, 7933 (2024).

[32] T. Meng, S. Florens, and P. Simon, Self-consistent description of Andreev bound states in Josephson quantum dot devices, Phys. Rev. B **79**, 224521 (2009).

[33] K. Grove-Rasmussen, H. I. Jørgensen, B. M. Andersen, J. Paaske, T. S. Jespersen, J. Nygård, K. Flensberg, and P. E. Lindelof, Superconductivity-enhanced bias spectroscopy in carbon nanotube quantum dots, Phys. Rev. B **79**, 134518 (2009).

[34] R. S. Deacon, Y. Tanaka, A. Oiwa, R. Sakano, K. Yoshida, K. Shibata, K. Hirakawa, and S. Tarucha, Tunneling spectroscopy of Andreev energy levels in a quantum dot coupled to a superconductor, Phys. Rev. Lett. **104**, 076805 (2010).

[35] E. J. Lee, X. Jiang, M. Houzet, R. Aguado, C. M. Lieber, and S. De Franceschi, Spin-resolved Andreev levels and parity crossings in hybrid superconductor–semiconductor nanostructures, Nat. Nanotechnol. **9**, 79 (2014).

[36] A. Jellinggaard, K. Grove-Rasmussen, M. H. Madsen, and J. Nygård, Tuning Yu-Shiba-Rusinov states in a quantum dot, Phys. Rev. B **94**, 064520 (2016).

[37] T. Yokoyama, M. Eto, and Y. V. Nazarov, Anomalous Josephson effect induced by spin-orbit interaction and Zeeman effect in semiconductor nanowires, Phys. Rev. B **89**, 195407 (2014).

[38] B. van Heck, J. I. Väyrynen, and L. I. Glazman, Zeeman and spin-orbit effects in the Andreev spectra of nanowire junctions, Phys. Rev. B **96**, 075404 (2017).

[39] L. Tosi, C. Metzger, M. F. Goffman, C. Urbina, H. Pothier, S. Park, A. L. Yeyati, J. Nygård, and P. Krogstrup, Spin-orbit splitting of Andreev states revealed by microwave spectroscopy, Phys. Rev. X **9**, 011010 (2019).

[40] F. Hassler, G. Catelani, and H. Bluhm, Exchange interaction of two spin qubits mediated by a superconductor, Phys. Rev. B **92**, 235401 (2015).

[41] L. Gonzalez Rosado, F. Hassler, and G. Catelani, Long-range exchange interaction between spin qubits mediated by a superconducting link at finite magnetic field, Phys. Rev. B **103**, 035430 (2021).

[42] T. A. Baart, T. Fujita, C. Reichl, W. Wegscheider, and L. M. K. Vandersypen, Coherent spin-exchange via a quantum mediator, Nat. Nanotechnol. **12**, 26 (2017).

[43] F. Borjans, X. Croot, X. Mi, M. Gullans, and J. Petta, Resonant microwave-mediated interactions between distant electron spins, Nature (London) **577**, 195 (2020).

[44] I. Kulesh and S. L. D. ten Haaf, Data repository accompanying "Flux-controlled two-site Kitaev chain", 10.5281/zenodo.13730031.